LAWRENCE
LIVERMORE
NATIONAL
LABORATORY

LLNL-JRNL-430513

The Surface-Pressure Signature of Atmospheric Tides in Modern Climate Models

C. Covey, A. Dai, D. Marsh, R. S. Lindzen

May 4, 2010

Journal of the Atmospheric Sciences

Disclaimer

This document was prepared as an account of work sponsored by an agency of the United States government. Neither the United States government nor Lawrence Livermore National Security, LLC, nor any of their employees makes any warranty, expressed or implied, or assumes any legal liability or responsibility for the accuracy, completeness, or usefulness of any information, apparatus, product, or process disclosed, or represents that its use would not infringe privately owned rights. Reference herein to any specific commercial product, process, or service by trade name, trademark, manufacturer, or otherwise does not necessarily constitute or imply its endorsement, recommendation, or favoring by the United States government or Lawrence Livermore National Security, LLC. The views and opinions of authors expressed herein do not necessarily state or reflect those of the United States government or Lawrence Livermore National Security, LLC, and shall not be used for advertising or product endorsement purposes.

The Surface-Pressure Signature of Atmospheric Tides in Modern Climate Models

Curt Covey

Program for Climate Model Diagnosis and Intercomparison, Lawrence Livermore National Laboratory, Livermore, CA

Aiguo Dai and Dan Marsh

National Center for Atmospheric Research, Boulder, CO

Richard S. Lindzen

Massachusetts Institute of Technology, Cambridge, MA

Submitted to *The Journal of the Atmospheric Sciences* 12 May 2010

Revised 14 September 2010

Corresponding author address: Curt Covey, LLNL Mail Code L-103, 7000 East Avenue, Livermore, CA 94550
E-mail: covey1@llnl.gov

LLNL-JRNL-430513

ABSTRACT

Although atmospheric tides driven by solar heating are readily detectable at Earth's surface as variations in air pressure, their simulations in current coupled global climate models have not been fully examined. This work examines near-surface pressure tides in climate models that contributed to the most recent assessment report of the Intergovernmental Panel on Climate Change (IPCC); it compares them with tides both from observations, and from the Whole-Atmosphere Community Climate Model (WACCM) which extends from Earth's surface to the thermosphere. Surprising consistency is found among observations and all model simulations, despite variation of the altitudes of model upper boundaries from 32 to 76 km in the IPCC models and 135 km for WACCM. These results are consistent with previous suggestions that placing a model's upper boundary at low altitude leads to partly compensating errors—reducing the forcing of the tides by ozone heating, but also introducing spurious waves at the upper boundary, which propagate to the surface.

1. Introduction

Atmospheric tides are important features of middle- and upper-atmosphere structure and circulation. At the surface, the tides are significant parts of the day-night variations in both climate observations and simulations (Dai and Trenberth, 2004, Woolnough et al. 2004). In the tropics—and in mid-latitudes after baroclinic waves are removed from consideration—the primary observed day-to-night variation of surface pressure is a semidiurnal (twice-a-day) cycle despite the obvious diurnal (once-a-day) cycle of surface temperature. Resolution of this apparent paradox invokes the fact that atmospheric tides are mainly excited above the surface. Thus wave propagation from the altitudes of tidal excitation down to the surface must be considered in evaluation of surface pressure variations (Chapman and Lindzen 1970, Hagan et al. 2004).

Solar heating is the primary driver of atmospheric tides. Gravitationally driven atmospheric tides, analogous to ocean tides, are about 20 times weaker than thermally driven atmospheric tides (e.g. Fig. 2L.6 in Chapman and Lindzen 1970). The gravitational tides are distinguishable from thermal tides because they are primarily driven by the Moon and thus appear in harmonics of a lunar day, 24.8 hours. If solar heating is decomposed into Fourier components $\exp(i(s\lambda + \sigma\Omega t))$, where λ is longitude, s is zonal wavenumber, t is time, $\Omega = 2\pi / (24 \text{ hours})$, and σ is normalized frequency, then both diurnal ($s = \sigma = 1$) and semidiurnal ($s = \sigma = 2$) components migrating with the

apparent motion of the Sun across the sky are significant. Linear responses to these components of solar hearing are often referred to as "migrating tides."

Even though most of the solar energy flux absorbed by Earth is deposited near the surface, peak atmospheric heating per unit mass at large scales occurs in the middle atmosphere via absorption of solar ultraviolet (UV) radiation by ozone. Most of the diurnal harmonic of ozone heating goes into a vertically trapped tidal mode (Chapman and Lindzen 1970, Forbes 1995). Diurnal modes that propagate down to the surface do so with vertical wavelengths < 30 km, allowing destructive interference in the forcing layer. However, the main semidiurnal-tide mode (Hough function (2, 2)) propagates vertically with wavelength > 300 km (e.g. Table 1 in Forbes 1995). Thus the semidiurnal tide is primarily excited in a broad range of altitudes around 50 km by ozone heating and effectively propagates to the surface. This explanation of the semidiurnal cycle of surface pressure came long after it was observed and only after the thermal structure and wave dynamics of the middle atmosphere was understood (Chapman and Lindzen 1970).

Given this explanation, one would expect to find surface-pressure tides in the output of any atmospheric general circulation model (GCM) that includes the ozone layer. Tides were indeed found by Hunt and Manabe (1968) in a very early GCM with enhanced vertical resolution and domain (18 vertical levels extending to 38 km altitude, comparable to modern climate-oriented GCMs). At the same time, however, Lindzen et

al. (1968) pointed out that spurious resonances will occur in a model atmosphere with an artificial "top." Much later, Zwiers and Hamilton (1986) examined their GCM's output for tides and concluded that compensating errors were at work: tidal amplitude was diminished by the model's omission of much of the ozone heating, but enhanced by the model's rigid-lid upper boundary condition, which introduced spurious reflected waves that propagated down to the surface. The result was a fortuitously accurate tide simulation. Recently Hamilton et al. (2008) examined output from the Atmospheric Model for the Earth Simulator (with its top at about 60 km altitude) and concluded that "simulated amplitudes of the semidiurnal oscillation [of surface pressure] have an overall enhancement of 25% over those observed, a deficiency which is reasonably attributable to the effects of the upper boundary condition in the model."

This study examines the surface-pressure signature of atmospheric tides in GCMs that contributed output to the most recent assessment report (AR4) of the Intergovernmental Panel on Climate Change (IPCC; Solomon et al. 2007). We confine our attention to near-surface pressure because this field is well observed, and because the primary database of IPCC AR4 model output (Meehl et al. 2007) contains only near-surface fields in its high-time-frequency output.

The IPCC coupled models were developed for climate-change simulations. Diurnal and semidiurnal variations in individual GCMs have been analyzed previously (e.g., Zwiers and Hamilton 1986; Lieberman et al. 1994; Dai and Trenberth 2004; Chang et al.

2008; Hamilton et al. 2008) but a systematic comparison of surface pressure tides in the IPCC AR4 models has not been done. Although the tides are a linear response to well-known forcing, the limited vertical domain of models may introduce errors in tidal simulations, as noted above. Also—as discussed by Dai and Trenberth (2004) and in Section 2 below—the design of most coupled ocean-atmosphere climate models, as well as atmospheric GCMs run with prescribed sea surface temperatures (SSTs) as a lower boundary condition, leads to underpredicted or nonexistent diurnal variations in their SSTs, which can result in reduced diurnal cycles in surface air temperature and pressure over the oceans in these models.

We also examine the tides in output from the Whole Atmosphere Community Climate Model (WACCM). Both the original version, without interactive atmospheric chemistry (WACCM-1; Sassi et al. 2002) and the most recent version, including chemistry (WACCM-3; Richter et al. 2008) are considered. Although it is a full atmospheric GCM including the surface and troposphere, WACCM was developed for studying the middle and upper atmosphere. At these altitudes, tidal oscillations are prominent in the wind and temperature fields from both WACCM and observations (Chang et al. 2008). However, WACCM's surface output has not been previously examined for the tides.

2. Data sources

The most recent analysis of global observations of surface-pressure tides (Dai and Wang 1999) is used in this study. This analysis included data from weather stations, commercial ships, and ocean buoys during the period 1976 – 1997. High-time-frequency (3-hourly) output from climate models was obtained from readily available sources. WACCM-1 output was downloaded from the National Center for Atmospheric Research community data portal (http://cdp.ucar.edu). WACCM-3 output was provided by the WACCM Working Group of the Community Climate System Model (CCSM) consortium; membership in this and other CCSM Working Groups is open to all interested scientists (see http://www.ccsm.ucar.edu/working_groups/WACCM). IPCC AR4 model output was downloaded from archives of the Coupled Model Intercomparison Project, phase 3 (CMIP3; Meehl et al. 2007). Diurnal and semidiurnal harmonics of the 3-hourly model output were obtained directly by Fast Fourier Transforms (FFTs) of the time series at each grid point. No interpolation of output from the original model grids was done unless required for statistics comparing different model results and observations. This procedure differs somewhat from the method used by Dai and Wang (1999) who averaged pressure data from 1976-1997 at each location to form a composite day-night cycle before fitting diurnal and semidiurnal curves to the 3-hourly composite diurnal data.

Table 1 gives names and key features of the models examined in this study. All 11 IPCC models that contributed 3-hourly data to CMIP3 are included, except for 2 models whose 3-hourly output in the database was problematic (e.g. only recorded once every 6 hours). Three of the 9 models we examined had a simple error in their recorded 3-hourly time coordinate values. After consulting the model developers, we added 1.5 hours to both GISS-EH and GISS-ER times, and we subtracted 4.5 hours from INM-CM3.0 times, to correct these errors. Table 1 shows that the IPCC models have top boundaries located between 32 and 76 km altitude, and they place 1 to 9 levels in the ozone-heating layer. Both WACCM versions have a top at 135 km altitude and place 23 levels in the ozone-heating layer. We define "the ozone-heating layer" as the 30 – 70 km altitude range, where most of the heating per unit mass occurs in the real world (e.g. Fig. 3.2 in Chapman and Lindzen 1970; it produces the well-known temperature maximum at the stratopause, ~50 km altitude). As discussed below, ozone heating in the models may occur at lower levels.

All of the IPCC models were driven by incoming solar energy flux at the top of the atmosphere together with observed greenhouse gas and aerosol concentrations for the late 20th century; they calculated SST and sea ice interactively as part of a coupled ocean-atmosphere GCM. Standard practice in these simulations is to couple the ocean and atmosphere once a day using daily mean values (e.g. Washington et al. 2009) thereby suppressing diurnal variations in SST. Six of the 9 models were also driven by

observed late-20th century monthly mean SSTs (again without diurnal variations) and sea ice concentration fields imposed as a lower boundary condition; these numerical experiments are called AMIP runs after the Atmosphere Model Intercomparison Project (Gates et al. 1998). WACCM-3 simulations are AMIP runs, and WACCM-1 simulations are AMIP-like runs forced by a climatological mean seasonal cycle of sea surface temperature (without diurnal variations) and sea ice for the late 20th century.

CMIP requested that IPCC models provide AMIP 3-hourly output for the year 2000 and coupled ocean-atmosphere 3-hourly output for years 1991 – 2000 inclusive. INM-CM3.0 however, provided coupled ocean-atmosphere 3-hourly output (as well as AMIP output) only for the year 2000. WACCM-3 provided output for years 1990 – 2000 inclusive. Therefore, in order to maximize consistency among the different model output datasets, we focus on year 2000 from all of the IPCC models and from WACCM-3. For these models, results shown below pertain to year 2000 unless noted otherwise. For WACCM-1, results are from an arbitrary "Year 1" since this model's output does not match any particular calendar years. Thus our model output pertains to a narrower and somewhat later interval of time (namely only January and July of 2000) than the observations from Dai and Wang (1999), which cover years 1976 – 1997. Interannual variations of the surface-pressure tides are relatively small, however, in contrast to the large interannual variations of the tides in the middle atmosphere (see Appendix).

With the exception of initial screening results shown in Table 1, we applied all FFTs on 32 days of model output (with 24 hr / 3 hr = 8 time points per day) for the months of January or July, with 1-day extensions into adjacent months to produce a number of time points equal to an exact power of 2, thereby saving computer time. Thus our model-simulated output approximately pertains to January or July, while the observed data is compiled for full seasons, i.e. December – January – February and June – July – August.

A far more significant inconsistency arises from a limitation of the CMIP3 database. It contains sea-level pressure (PSL) but not surface pressure (PS) in its 3-hourly output, whereas the observations are derived from PS, the more fundamental quantity. In theory a simple formula inter-converts PS and PSL (e.g. Section 3.2.4 in Wallace and Hobbs 2006) but in practice each model applies its own idiosyncratic procedure, using data that is not generally saved. Therefore it is not possible to convert PSL back to PS in the 3-hourly CMIP3 model output. Both PS and PSL output are available from WACCM-1 at 3-hourly frequency, however. We use this output to assess the magnitude of the problem and to investigate a partial solution.

Figure 1 compares January PS-based tide amplitudes from WACCM-1, the corresponding PSL-based amplitudes, and the same PSL-based amplitudes with areas > 1 km in elevation omitted. Table 2 presents associated comparison statistics in both January and July. Aliasing problems are most apparent for the diurnal harmonic,

probably due to the strong diurnal cycle of land surface temperature affecting conversion of PS to PSL. For the diurnal tide (Fig. 1a) switching from PS to PSL boosts amplitudes by up to a factor of 6 over land, particularly at high elevations where the concept of equivalent sea-level pressure is most dubious. Application of the < 1 km constraint removes nearly all of the egregiously high (> 360 Pa) PSL-based amplitudes and reduces the global mean overestimate from about a factor of 2 down to 20 – 30%. Nevertheless, many land areas remain where PSL-based amplitudes are several times higher than their PS-based counterparts, and the root-mean-square difference between PS- and PSL-based amplitudes, while reduced from about 95 to 30 – 40 Pa, is still comparable to the global mean PS-based amplitude (39 Pa for January). For the semidiurnal tide (Fig. 1b) the < 1 km constraint removes essentially all of the problematic areas. Under this constraint, statistics comparing PS- with PSL-based semidiurnal amplitudes show global means within 5% of each other, correlations > 0.99, and r.m.s. differences < 10% of the global mean.

In short, for the semidiurnal tide, removing areas > 1 km in elevation from consideration may remove most of the PS vs. PSL inconsistency when comparing IPCC model simulations with observations, while retaining substantial land as well as ocean areas in the comparison. For the diurnal tide, however, this constraint fails to eliminate a number of problematic land points, and the global mean discrepancy is not reduced below 20 – 30%. A more severe constraint (perhaps eliminating all land areas from

consideration) is needed for accurate comparison of diurnal tide simulations with observations. On the other hand, we wish to make at least some inspection of the model-simulated diurnal tide over land. Also, for WACCM output the PS-based tides are available and there is no obvious reason to impose any geographic constraint. As a simple compromise of these conflicting interests, we place the < 1 km constraint on all IPCC PSL-based results below, while for WACCM output we include the full geographic coverage of PS-based results. In the Discussion section we also present PSL-based WACCM results with the < 1 km constraint imposed, allowing a consistent comparison of WACCM's accuracy with the IPCC models' accuracy.

3. Results

a. Tidal amplitude

In addition to model characteristics, Table 1 shows results of our first screening test of model output. We took an area average in the vicinity of Jakarta (formerly Batavia) in Indonesia from both the models and observations. The classic observed signature of the tides—shown for example in Fig. 1.1 of Chapman and Lindzen (1970)—is a semidiurnal variation of surface pressure at this location. Chapman and Lindzen's figure shows data taken at Batavia during the first half of November 1919. The amplitude of surface pressure variation is ~100 Pa and the phase has maxima at about 10 AM and 10 PM local solar time. We examined the corresponding half-month in the

models (taken from "year 1" in WACCM-3, year 2000 in INM-CM3.0, and year 1991 in all other models) and the September – October – November season in the modern observations (Dai and Wang 1999). These observations confirm that the 1919 Batavia data are representative of the tropics in all seasons (see figures discussed below). The modern observations, however, give a smaller semidiurnal harmonic amplitude than older observations do for the full region considered in Table 1 (Haurwitz 1956; see Fig. 2S.3 in Chapman and Lindzen 1970). The smaller amplitude arises from inclusion of more stations in this region.

Table 1 shows that most of the models obtain the correct diurnal harmonic amplitude at Jakarta to within ±20%, but all of them overestimate the amplitude of the semidiurnal harmonic, some by nearly a factor of 2. Thus the models agree with observations that the semidiurnal harmonic dominates surface-pressure variations, but they overestimate its dominance. The models generally put the maximum near-surface pressure earlier than observed for the diurnal harmonic, but later than observed (by ~1 hour) for the semidiurnal harmonic. (A phase error in the semidiurnal harmonic appears with opposite sign in "classical" linear calculations, probably because they neglect release of latent heat in the tropical atmosphere (Lindzen 1978)). Also, results from the coupled ocean-atmosphere 20th century experiments exhibit close agreement with results from the AMIP experiments in Table 1. Thus the surface-pressure tides are not sensitive to SST errors in the coupled ocean-atmosphere simulations, or to

interannual SST variations. This conclusion is consistent with the classical theory of the migrating tides, though non-migrating components include sea breezes and low-level jets that are sensitive to surface temperature distributions. Finally, the table shows that for Jakarta—which lies near sea level—there is essentially no difference between amplitudes and phases derived from PS and PSL, as expected.

Figures 2 and 3 map diurnal and semidiurnal tide amplitudes, respectively, from two of the IPCC models, from WACCM-3, and from the observations. To save space, only data for the month of January is shown in the figures. Table 3 presents global statistics for both January and July comparing the same two IPCC models and both WACCM versions with the observations. The two IPCC models selected are INM-CM3.0, which has the lowest model top (32 km) and CNRM-CM3, which has the highest model top (76 km). Tide amplitude maps from the other IPCC models (not shown here) have similar appearance. Later sections of this paper will present results from all 9 of the IPCC models that provided appropriate 3-hourly output.

Comparison of the WACCM simulations with observations is straightforward because both are available in terms of surface pressure. The resulting statistics are quite similar between the two WACCM versions. From this point of view the most noticeable discrepancy between WACCM and observations is that both model versions underestimate the diurnal tide amplitude over large areas, particularly over the ocean (top panel of Fig. 1a and bottom two panels of Fig. 2) so that the global mean of model /

observed amplitude ratio lies in the range 0.6 – 0.7 (Table 3). As noted in the previous section, standard methods of running most climate models including WACCM underestimate diurnal SST variations. WACCM's semidiurnal tide amplitude, on the other hand, compares with observations more favorably. The global mean of model / observed semidiurnal amplitude ratio lies in the range 0.9 – 1 while the simulated global mean (77 Pa) is slightly larger than the observed global mean (73 Pa). The amplitude pattern correlation with observations is 0.6 – 0.7 for the diurnal harmonic and > 0.9 for the semidiurnal harmonic. The root-mean-square difference between WACCM and observed amplitudes is an appreciable fraction of the global mean (~27 Pa / 37 Pa) for the diurnal harmonic and a much smaller fraction of the global mean (~20 Pa / 77 Pa) for the semidiurnal harmonic.

Examination of the top panel of Fig.1a and the bottom two panels of Fig. 2 also shows that WACCM-1's excessive values of diurnal amplitude over tropical continents are removed in WACCM-3. Since the diurnal tide over land has a large influence from surface heating, this improvement may be due to changes in the lower-atmosphere climate physics (from the Community Climate Model version 3 in WACCM-1, to the Community Atmosphere Model version 3 in WACCM-3).

For the IPCC models, comparison with observations is not straightforward because—as noted above—the CMIP3 database contains PSL but not PS in its 3-hourly output, whereas the observations are derived only from PS; therefore we consider only

areas < 1 km in elevation in the IPCC model output. Under this constraint Table 3 shows that for the diurnal harmonic amplitude, CNRM-CM3 and INM-CM3.0 attain correlations with observed values that are generally higher than WACCM's, which do not suffer from the problem of comparing PSL with PS but do suffer the handicap of comparing at all points on Earth's surface including high elevations. The global means of model / observed diurnal amplitude ratios lie in the range 0.8 – 1.0 for CNRM-CM3 and INM-CM3.0, higher than for WACCM, but Fig. 2 shows that the two IPCC models achieve this "improvement" by overestimating diurnal tide amplitude in the interiors of tropical continents. The problem is worse for INM-CM3.0, the model with the lowest top (up to a factor of 3 overestimate) than it is for CNRM-CM3.0, the IPCC model with the highest top (up to a factor of 2 overestimate). Much of this discrepancy may be explained by our comparison of PSL-based model output with PS- based observations, however (see Fig. 1 and Table 2). The diurnal amplitudes from the two selected IPCC models are generally underestimated over oceans, as in WACCM's results.

Turning to the semidiurnal harmonic, the previous section noted that the < 1 km elevation constraint removes many of the problematic aspects of comparing PSL-based tide simulations with PS-based observations, and amplitude maps from INM-CM3.0 and CNRM-CM3 show better agreement with both WACCM and observations (Fig. 3). Comparison statistics (Table 3) show global mean IPCC model / observed amplitude ratios in the range 0.91 – 0.99 and correlation values ~0.9, about the same as for

WACCM-1 and WACCM-3. The r.m.s. differences between the two IPCC models and observations lie in the range 19 – 24 Pa, compared with the range 19 – 22 Pa for WACCM-1 and WACCM-3. The maximum value of semidiurnal amplitude, however, is ~180 – 190 Pa for the two IPCC models, compared with 160 Pa for WACCM-3, so WACCM's maximum is closer to the observed value (140 Pa).

b. Tidal phase

Figures 4 – 5 show times of maximum pressure for the diurnal and semidiurnal harmonics, respectively, in the same models and month (January) as in Figs. 2 – 3. Figures 4 – 5 show that in the tropics, the observed times of maximum are about 6 AM for the diurnal harmonic and 10 AM / PM for the semidiurnal harmonic; at higher latitudes the phases are unclear. Simulated diurnal phases from both IPCC models and WACCM-3 are roughly consistent with the observed diurnal phase in the tropics, where amplitude is greatest, but the model-simulated phase varies more smoothly from one location to another than the observed phase. Agreement between the models and observations is more evident for the phase of the semidiurnal tide (Fig. 5) although the observations again exhibit more spatial variation at higher latitudes than the models. It is difficult to determine how much of this discrepancy is due to errors in the models, as opposed to noise in the observations. An unrealistically smooth distribution would suggest underrepresentation of the non-migrating tides in the GCM calculations.

Extracting the migrating components of the tides allows a more precise quantification of their phase, as shown below.

c. Zonal wavenumber decomposition

Classical linear calculations of the migrating (Sun-synchronous) components of the tides provide a good approximation to the observed surface-pressure variations, as well as physical insights not easily obtained from GCMs (Chapman and Lindzen 1970). Therefore, it is worthwhile to isolate the migrating components from the GCM output. The first step in this process is Fourier analysis in the longitude dimension, producing tidal amplitude as a function of latitude and zonal wavenumber s from tidal amplitude as a function of latitude and longitude.

Figures 6 – 7 show results for the diurnal ($\sigma = 1$) and semidiurnal ($\sigma = 2$) harmonics respectively. These figures display the same models and month (January) as in Figs. 2 – 5. The most obvious feature of Figs. 6 – 7 is the concentration of tidal amplitude in the migrating component, $s = \sigma$. This concentration of amplitude is more exaggerated in the models than in the observations. For example, WACCM-3 produces a migrating diurnal tide at the Equator that is stronger than its observed counterpart (Fig. 6) even though the overall global mean amplitude of WACCM-3's diurnal harmonic is less than observed (Fig. 2). Figure 7 indicates that the models overestimate the migrating component of the semidiurnal tide by an even larger factor (about a

factor of 2). In addition, Fig. 7 shows a small but distinct stationary (s = 0) semidiurnal tide with multiple peaks in latitude in the model simulations, but not in the observations.

Figure 8 shows diurnal and semidiurnal tidal amplitudes for both January and July as a function of zonal wavenumber s at the Equator from all IPCC models providing appropriate output, from WACCM-3, and from observations. The figure shows that many conclusions drawn from previous figures for INM-CM3.0 and CNRM-CM3 generalize to all the other IPCC models. All models and observations qualitatively agree that the semidiurnal harmonic amplitude is larger than the diurnal harmonic, and that the migrating ($s = \sigma$) component dominates both harmonics. Quantitatively, however, the migrating component simulated by every model including WACCM-3 has larger amplitude than observed. WACCM-3's amplitude is consistently at the lower end—i.e. the more accurate end—of the range of model-simulated values. This range varies between about 20% greater and 100% greater than observed for the diurnal harmonic, and between about 70% greater and 150% greater than observed for the semidiurnal harmonic. As noted above, however, much of the overestimate of diurnal tide amplitude by the IPCC models in this study is due to data limitations, which lead to an inconsistent comparison of PS with PSL. Also, observational uncertainty might reasonably be put at 10 – 20%, in which case WACCM and several of the IPCC models would lie within the observational "error bars."

A second message of Fig. 8 is that there is little difference between January and July in the equatorial tidal amplitudes, for either the models or the observations.

Figure 9 shows, for the migrating ($s = \sigma$) tide components only, phase as a function of latitude. As in Fig. 8, the diurnal and semidiurnal harmonics for both January and July are shown from all available IPCC model output and from WACCM-3. Observations are not shown, however. A more extensive analysis of observations than hitherto published would be necessary in order to say which of the models provides the most accurate phase in Fig. 9. Recall, however, that the lower-right panels of Figs. 4 – 5 display the observed local solar times of maximum surface pressure for all zonal wavenumbers combined, which Fig. 8 shows is dominated by the migrating component. Figs. 4 – 5 show that in the tropics the observed times of maximum are about 6 AM for the diurnal harmonic and 10 AM / PM for the semidiurnal harmonic. Figure 9 shows that diurnal migrating components from all of the models exhibit maximum pressures between 4 and 8 AM equatorward of ±30° latitude. Poleward of these latitudes, especially in the winter hemisphere, the phase of the weak diurnal tide is not well defined. The stronger semidiurnal tide exhibits well-defined phases up to at least ±40° latitude in all of the models. Equatorward of these latitudes, the times of semidiurnal maxima lie between about 9:30 and 11 AM / PM for all models. Thus the model-simulated phases are roughly consistent with observations. Note, however, that the differences between different models—up to about 4 hours for the diurnal harmonic

and 1.5 hours for the semidiurnal harmonic—amount to 60° and 45° variations in phase, respectively, so at least a subset of the models are exhibiting significant phase errors.

One possibly noteworthy feature of the semidiurnal migrating tide in two of the models (GFDL-CM2.1 and MIROC3.2 (medres)) is a systematic decrease in the time of maximum pressure from the summer hemisphere to the winter hemisphere. Because this feature is determined by the high-latitude behavior of the tides, where the signal is irregular and weak, it seems unlikely that observations can assess its validity.

4. Discussion

Unlike the IPCC climate models, WACCM was developed for middle- and upper-atmospheric research. At these altitudes the atmospheric diurnal tide attains large amplitude (Pirscher et al. 2010) and becomes a significant part of atmospheric motion and temperature variability; here WACCM produces simulations in general agreement with past tidal studies (Chang et al. 2008). WACCM also includes a complete lower atmosphere underneath its middle and upper atmosphere. This study shows that WACCM reproduces the major observed features of the surface-pressure signature of the tides. For the semidiurnal tide—the dominant harmonic in both simulations and observations of surface pressure—WACCM's global mean amplitude is within ~10% of observed, its pattern correlation with observations exceeds 0.9, and its r.m.s. difference

from observations is about 30% of the observed global mean and 15% of the observed maximum value (Table 3; Fig. 3).

Most of the IPCC models exclude at least part of the ozone-absorption altitude range (~30 – 70 km) that is thought primarily responsible for driving the surface-pressure tide. This does not mean that ozone heating is totally missed by the models, because there are abundant ozone molecules at altitudes < 30 km to absorb the same UV radiation. Thus models with low tops could produce a total column-integrated ozone heating in W m^{-2} similar to that in the real world, albeit at lower altitudes. But the same heating in W m^{-2} deposited at lower altitudes implies less heating per unit mass: if the heating occurs where air density is ρ_H, then the wave amplitude (perturbation temperature, wind velocity, etc.) at this location is proportional to ρ_H^{-1}. The wave amplitude at the surface is changed by a factor $(\rho_H/\rho_S)^{1/2}$, where ρ_S is air density at the surface. Multiplying this factor by ρ_H^{-1} implies that the wave amplitude at the surface varies as $\rho_H^{-1/2}$, so depositing the same heating in W m^{-2} at a lower level (where ρ_H is larger) diminishes the surface response. This scaling argument is qualitatively consistent with the results of Zwiers and Hamilton (1986). Their GCM placed its top boundary at 10 mb, the same pressure level as the lowest top among the models studied here (INM-CM3.0). As noted by Hamilton et al. (2008), Zwiers and Hamilton's separate linear calculations imply that wave reflection at their GCM's top enhanced the

semidiurnal tide amplitude by ~30%, largely canceling a 40% amplitude reduction due to altered ozone heating.

A similar cancelation of errors in low-top models may lead to comparable tide simulations across a wide range of vertical domains. In the present study the PS- vs. PSL-inconsistency between IPCC model output and observations is an important caveat, but for the dominant semidiurnal harmonic, the inconsistency is largely remedied by excluding areas > 1 km in elevation (Fig. 1b and Table 2). Under this constraint both the amplitude maps (Fig. 3) and the comparison statistics (Table 3) imply that the two selected IPCC models (with tops at 32 and 76 km) provide semidiurnal tide simulations comparable in quality to WACCM (with top at 135 km) though not quite as good. The model-observed pattern correlations are all ~0.9, but the maps show that the two IPCC models make a more severe overestimate than WACCM of the semidiurnal tide maximum near the Equator. The semidiurnal phase from the two IPCC models is a fair match to WACCM's (and to observations equatorward of ± 30° latitude; see Fig. 5).

To summarize the surface-pressure signature of atmospheric tides in WACCM-1, WACCM-3 and the IPCC models, Fig. 10 plots the three statistical metrics of model-observed agreement appearing in Table 3 against the two model characteristics appearing in Table 1 (altitude of model top; number of levels with significant ozone absorption of solar radiation in the real world). Thus the figure consists of six frames. In

each frame a model-simulated tide harmonic is represented by a single point. WACCM points appear in a single column on the extreme right of each frame, indicating a much higher model top and a much better resolution of ozone absorption than any of the IPCC models. Most points (filled circles) compare PSL-based model tides with PS-based observed tides excluding areas > 1 km in elevation. The remaining points (asterisks) show a global comparison of PS-based model tides with PS-based observed tides, which is available only from the two WACCM versions. For WACCM-1, which provided both PS and PSL output at high time-frequency, we also show the comparison of PSL-based model tides with PS-based observed tides with areas > 1 km in elevation excluded (filled circles in right-most columns). These points provide a consistent comparison of WACCM's accuracy with the IPCC models' accuracy.

The most striking feature of Fig. 10 is the absence of any obvious connection between simulation quality, as measured by our comparison statistics, and either (1) the vertical extent of the models or (2) vertical resolution in the altitude range 30 – 70 km. This result is consistent with the "canceling errors" interpretation of model behavior discussed above. The issue is complicated by the possibility that some GCMs omitting the altitude range where ozone heating occurs in the real world may absorb solar UV radiation lower down, while others may remove the radiation before it reaches the top of the model. Unfortunately the CMIP3 / IPCC AR4 database of climate model output does not include heating rates, so there is no simple way to inter-compare ozone

heating among the IPCC models. Also, modern GCMs generally include parameterizations that reduce wave reflection at the model top. The standard "sponge layer" with a constant time-scale for wave damping, however, is less effective for tides than for planetary waves because the latter have longer periods.

In contrast, WACCM with its top at 135 km includes all tidal forcing but produces semidiurnal amplitudes generally lower (i.e. in better accord with observations) than the IPCC models. Evidently any spurious enhancement of the tides by wave reflection at the upper boundary is much reduced in WACCM. Indeed, Fig. 10 shows that the globally averaged ratio of simulated to observed tidal amplitude is about 0.8 – 1.0 in WACCM but > 1 in most of the IPCC models when comparing simulations and observations consistently (i.e. PSL-based simulations vs. PS-based observations: filled circles). Figure 10 also shows that the model-observed pattern correlation of tide amplitudes is ~0.85 – 0.95 for the semidiurnal harmonic and ~0.65 – 0.75 for the diurnal harmonic. This result occurs across the full range of model-top altitudes from 32 km (INM-CM3.0) to 135 km (WACCM).

5. Conclusion

This study documents a comparable quality of surface-pressure tide simulations among 9 very different climate models—many of which exclude the altitude range that is most important to real-world tide forcing—and a "whole atmosphere" model that

was designed to include the tides. Our results suggest errors that partly cancel in some of the models, at least in terms of the metrics we have chosen. This implication is consistent with previous studies that span the history of GCM simulation (Lindzen et al. 1968, Zwiers and Hamilton 1986, Hamilton et al. 2008) but generally have not influenced the development of climate-oriented GCMs. As such models extend their purview above the troposphere (a necessary condition for full assessment of solar effects on climate) the tides along with other important features of the middle atmosphere must be given more attention.

The cancelation of errors in GCMs with lower tops is not precise, of course. For example, many of the IPCC models overestimate tide amplitudes at the surface. Also, most of the models in Table 1 obtain maximum semidiurnal-tide pressure at local solar times later than observed. (Such phase errors may arise from radiation time-steps being much longer than dynamics time-steps, leading to inaccurate forcing of model dynamics during the time that radiative heating is held constant.) No doubt more detailed and more physically-based comparisons of surface tide simulations and observations would reveal additional distinctions among the IPCC models, and between the IPCC models as a group and WACCM. Inspecting the latitude dependence in terms of modes produced by the classical linear calculations (Hough functions) would provide additional insight, since each of the modes has a different vertical wavelength or e-folding distance. Indeed, plotting the migrating semidiurnal tide

amplitudes against latitude for all of the models (not shown here) results in a series of bell-shaped curves symmetric about the Equator, consistent with the fundamental semidiurnal Hough function ($s = n = 2$ in Table 1 and Fig. 7 of Forbes 1995). A more thorough assessment of model behavior in terms of the classical theory might also involve extracting the heating rates out of the GCMs and using them as input to linear calculations, as Zwiers and Hamilton (1986) did with one GCM. Detailed comparison of theory and observations in locally data-dense areas, as done by Hamilton et al. (2008), might also prove useful.

The next generation of the IPCC / CMIP database will include PS rather than PSL in its 3-hourly output (while retaining PSL in daily-mean output for studies of weather systems; see http://cmip-pcmdi.llnl.gov/cmip5/docs/standard_output.pdf). This will allow a much cleaner comparison between climate model simulations and observations of surface atmospheric tides than was possible in the present study. Finally, information about tidal behavior above the surface, even if only for a limited number of models and observations, offers great scope for better understanding the underlying processes, and for the use of classical theory to interpret model results. For example, Pirscher et al. (2010) studied the diurnal tide in the upper troposphere and lower stratosphere, obtaining about 20% greater amplitude from short-term numerical weather predictions compared with more direct observations using Global Positioning System (GPS) radio

occultations. This result may be related to our finding that most climate-oriented GCMs overestimate tide amplitude at the surface.

Acknowledgements

We are grateful to many colleagues for comments on preliminary accounts of these results, in particular to E. C. Cordero and S. Tesfai for correcting the list of model features, and to Robert E. Dickinson for discussion of tide forcing and propagation. We also thank Sabrina Fletcher and Alexandria Ballard for graphic art. We acknowledge the modeling groups, the Program for Climate Model Diagnosis and Intercomparison, and the World Climate Reasearch Program (WCRP) Working Group on Coupled Modelling for their roles in making available the WCRP CMIP3 multi-model dataset. Support of this dataset is provided by the Office of Science, U.S. Department of Energy. This work was performed in part under auspices of the Office of Science, US Department of Energy, by Lawrence Livermore National Laboratory under Contract DE-AC52-07NA27344, and in part at the National Center for Atmospheric Research, which is sponsored by the National Science Foundation.

References

Chapman, S., and R. S. Lindzen, 1970: *Atmospheric Tides*. D. Reidel, 200 pp. + ix.

Chang, L., S. Palo, M. Hagan, J. Richter, R. Garcia, D. Riggin, and D. Fritts, 2008: Structure of the migrating diurnal tide in the Whole Atmosphere Community Climate Model (WACCM). *Advances in Space Research*, **41,** 1398-1407.

Cordero, E. C., and P. M. de Forster, 2006: Stratospheric variability and trends in models used for the IPCC AR4. *Atmos. Chem. Phys.* **6,** 369-5380.

Dai, A., and J. Wang, 1999: Diurnal and Semidiurnal Tides in Global Surface Pressure Fields. *J. Atmos. Sci.*, **56,** 3874-3890.

Dai, A., and K. E. Trenberth, 2004: The diurnal cycle and its depiction in the Community Climate System Model. *J. Climate*, **17,** 930-951.

Forbes, J. M., 1995: Tidal and planetary waves. *The Upper Mesosphere and Lower Thermosphere: A Review of Experiment and Theory*. Geophysical Monograph 87, American Geophysical Union, 67-87.

Gates, W. L., and Coauthors, 1998: An overview of the results of the Atmospheric Model Intercomparison Project (AMIP I). *Bull. Amer. Meteor. Soc.*, **80,** 29-55.

Hagan, M. E., J. M. Forbes, and A. Richmond, 2003: Atmospheric tides. *The Encyclopedia of Atmospheric Sciences*, J. R. Holton, J. Pyle and J. A. Curry, Eds., Academic Press, 159-165.

Hamilton, K., and R. R. Garcia, 1984: Long-period variations in the solar semidiurnal atmospheric tide. *J. Geophys. Res*.**, 89**, 11,705–11,710, doi:10.1029/JD089iD07p11705.

Hamilton, K., S. C. Ryan, and W. Ohfuchi, 2008: Orographic effects on the solar semidiurnal surface tide simulated in a very fine resolution general circulation model. *J. Geophys. Res.*, **113,** D17114.

Haurwitz, B., 1956: The geographical distribution of the solar semidiurnal pressure oscillation. *Meteorol. Pap.,* **2,** New York University, 1-36.

Hunt, D. C., and S. Manabe, 1968: An investigation of thermal tidal oscillations in the Earth's atmosphere using a General Circulation Model. *Mon. Wea. Rev.*, **96,** 753-766.

Lieberman, R. S., C. B. Leovy, B. A. Boville, and B. P. Briegleb, 1994: Diurnal heating and cloudiness in the NCAR Community Climate Model (CCM2). *J Climate*, **7**, 869-889.

Lindzen, R.S., E.S. Batten, and J.-W. Kim, 1968: Oscillations in atmospheres with tops. *Mon. Wea. Rev.*, **96,** 133-140.

Lindzen, R.S., 1978: Effect of daily variations of cumulonimbus activity on the atmospheric semidiurnal tide. *Mon. Wea. Rev.*, **106,** 526-533.

Meehl, G.A, C. Covey, T. Delworth, M. Latif, B. McAvaney, J.F.B. Mitchell, R.J. Stouffer and K.E. Taylor, 2007: The WCRP CMIP3 multimodel dataset: A new era in climate change research. *Bull. Amer. Meteor. Soc.*, **88,**1383-1394.

Pirscher, B., U. Foelsche, M. Borsche, G. Kirchengast, and Y.-H. Kuo, 2010: Analysis of migrating diurnal tides detected in FORMOSAT-3/COSMIC temperature data. *J. Geophys. Res.*, **115,** D14108, doi:10.1029/2009JD013008.

Randall, D.A., and Coauthors, 2007: Climate Models and Their Evaluation. In: *Climate Change 2007: The Physical Science Basis*. Contribution of Working Group I to the Fourth Assessment Report of the Intergovernmental Panel on Climate Change, S., Solomon, D. Qin, M. Manning, Z. Chen, M. Marquis, K.B. Averyt, M.Tignor and H.L. Miller, Eds., Cambridge University Press, 589-662.

Richter, J., F. Sassi, R.R. Garcia, K. Matthes, and C.A. Fischer, 2008: Dynamics of the middle atmosphere as simulated by the Whole Atmosphere Community Climate Model, version 3 (WACCM3), *J. Geophys. Res.*, **113,** D08101, doi: 10.1029/2007JD009269.

Sassi, F.S., R.R. Garcia, B.A. Boville, and H. Liu, 2002: On temperature inversions and the mesospheric surf zone. *J. Geophys. Res.*, **107,** 4380, doi: 10.1029/2001JD001525.

Solomon, S., D. Qin, M. Manning, Z. Chen, M. Marquis, K.B. Averyt, M.Tignor, and H.L. Miller (eds.), 2007: *Climate Change 2007: The Physical Science Basis*. Contribution of Working Group I to the Fourth Assessment Report of the Intergovernmental Panel on Climate Change, Cambridge University Press, 996 pp. + viii.

Wallace, J. M., and P. V. Hobbs, 2006: *Atmospheric Science: An Introductory Survey*. 2nd. ed. Academic Press, 483 pp. + xvi.

Washington, W. W., L. Buja, and A. Craig, 2009: The computational future for climate and Earth system models: on the path to petaflop and beyond. *Phil. Trans. R. Soc. A*, **367,** 833-846.

Woolnough, S.J., J.M. Slingo, and B.J. Hoskins, 2004: The diurnal cycle of convection and atmospheric tides in an aquaplanet GCM. *J. Atmos. Sci.*, **61,** 2559-2573.

Zwiers, F. and K. Hamilton, 1986: Simulation of solar tides in the Canadian Climate Center General Circulation Model. *J. Geophys. Res.*, **91,** 11877-11896.

Appendix: Interannual Variation of the Surface-Pressure Tide

Interannual variations appear to be small in the GCM surface-pressure tides, especially for the semidiurnal harmonic. Figure A1 shows the ratio of the standard deviation to the mean of January diurnal and semidiurnal tide amplitudes from WACCM-3, taken over all 11 years provided. For the semidiurnal tide, this ratio is < 0.05 equatorward of latitudes ±30°, and it only attains values > 0.2 poleward of ±60°, where the tidal amplitude is not appreciable (Fig. 3 bottom panel). The observational study of Hamilton and Garcia (1984) is consistent with these model results, obtaining a ratio generally < 0.1 for the semidiurnal harmonic from 79 years of surface barometric data at "Batavia."

The ratio is greater for the diurnal tide, attaining values ~1 in many areas poleward of ±60°, but it remains < 0.4 almost everywhere in the tropics (Fig. 3 top panel). Thus interannual variations of the diurnal surface-pressure harmonic are non-negligible, though they are smaller than the interannual variability of diurnal tides in the middle atmosphere.

TABLE 1. Model characteristics and tidal near-surface pressure variations near "Batavia" (now Jakarta, 14°S-2°N, 97.5°E-112.5°E)

Source[a]			Diurnal harmonic		Semidiurnal harmonic	
	Model top[b]	Levs[c]	Amplitude [Pa]	Time of max [hrs LST]	Amplitude [Pa]	Time of max [hrs LST]
CNRM-CM3	0.05 hPa (76 km)	45 (8)	71.6	4:35	140.1	9:35
CNRM-CM3 AMIP			76.0	4:42	137.6	9:38
GFDL-CM2.0	3 hPa (35 km)	24 (1)	44.0	6:16	134.6	10:22
GFDL-CM2.1		24 (1)	61.0	5:46	131.1	10:39
GISS-EH	0.1 hPa (67 km)	20 (5)	70.4	4:15	176.2	10:35
GISS-ER		20 (5)	94.7	4:19	182.0	10:33
GISS-ER AMIP			77.6	4:54	175.3	10:09
INM-CM3.0	10 hPa (32 km)	21 (1)	65.1	5:08	144.9	10:04
INM-CM3.0 AMIP			73.8	3:47	147.6	10:03
MIROC3.2(hi-res)	0.3 hPa (45 km)	56 (5)	40.4	6:16	148.0	10:09
MIROC3.2(hi-res) AMIP			57.7	6:31	144.5	10:11
MIROC3.2(med-res)	0.1 hPa (67 km)	20 (1)	64.0	6:60	178.1	10:54
MIROC3.2(med-res)AMIP			62.4	7:34	163.2	10:52
MRI-CGCM3.2	0.4 hPa (54 km)	30 (7)	59.2	5:46	193.3	11:14
MRI-CGCM3.2 AMIP			49.0	5:38	175.6	10:57
WACCM-1 Jan climat.	4.5×10^{-6} hPa (135 km)	66 (23)	52.0	5:17	125.2	10:48
WACCM-1 Jan climat.			54.9	5:12	126.0	10:48
WACCM-1 Jul climat. PS			57.1	3:15	113.6	10:48
WACCM-1 Jul climat. PSL			59.4	3:17	114.3	10:47
WACCM-3 Jan AMIP PS			54.7	4:34	134.7	9:53
OBSERVATIONS			64.9	5:59	99.8	9:56

[a] Observations are surface pressure. Model output is sea-level pressure from IPCC, both sea-level pressure and surface pressure from WACCM-1, and surface pressure from WACCM-3. "climat." = AMIP-like run with repeating climatological mean seasonal cycle.

[b] Pressure at model top and corresponding approximate altitude. All models use pressure-based vertical coordinates: INM and MIROC use "sigma" ≡ pressure / (surface

pressure) throughout; the others use sigma at lower levels transitioning to pressure at higher levels.

[c] Total number of vertical levels, and (in parentheses) number of levels at altitudes with large solar UV absorption by ozone (30 km < z < 70 km). For IPCC models, see Figure 1 of Cordero and Forster (2006) for placement of vertical levels. Note that Cordero and Forster's compilation corrects an error in the MIROC3.2 (med-res) top altitude that appears in the IPCC Working Group 1's Table 8.1 (Randall et al. 2007). WACCM model levels from Richter et al. (2008) and references therein.

TABLE 2. Comparison of January and July surface pressure (PS) vs. sea-level pressure (PSL) tide amplitude maps simulated by WACCM-1

Harmonic	Month	Global average of PSL / PS ratio	PSL – PS correlation	PSL – PS r.m.s. difference [Pa]
Diurnal	January	2.26 unmasked*	0.487 unmasked	95.5 unmasked
		1.21 masked	0.894 masked	31.8 masked
Diurnal	July	1.90 unmasked	0.569 unmasked	94.4 unmasked
		1.31 masked	0.862 masked	37.0 unmasked
Semidiurnal	January	1.18 unmasked	0.932 unmasked	19.3 unmasked
		1.05 masked	0.994 masked	5.9 masked
Semidiurnal	July	1.04 unmasked	0.966 unmasked	11.7 unmasked
		1.00 masked	0.996 masked	4.0 masked

* "Unmasked" means that comparison is made over the entire surface area of Earth. "Masked" means that land areas with elevation > 1 km are excluded from the comparison.

TABLE 3. Comparison of observed surface-pressure tide amplitude with model-simulated tide amplitude from WACCM-1 and WACCM-3 (surface pressure output, unmasked) and from selected CMIP3 / IPCC AR4 models (sea-level pressure output, masked)*

Model	Harmonic	Month	Global mean of model / obs ratio	Model – obs correlation	Model – obs r.m.s. diff [Pa]
WACCM-1	Diurnal	January	0.676	0.724	28.3
WACCM-3			0.681	0.673	25.9
WACCM-1	Diurnal	July	0.682	0.672	27.7
WACCM-3			0.733	0.620	25.1
WACCM-1	Semidiurnal	January	0.952	0.936	21.3
WACCM-3			0.962	0.943	20.1
WACCM-1	Semidiurnal	July	0.924	0.907	19.3
WACCM-3			0.946	0.910	19.7
INM-CM3.0	Diurnal	January	0.808	0.703	39.6
INM-CM3.0	Diurnal	July	0.944	0.739	39.9
INM-CM3.0	Semidiurnal	January	0.920	0.912	20.6
INM-CM3.0	Semidiurnal	July	0.914	0.885	19.4
CNRM-CM3	Diurnal	January	0.843	0.733	33.4
CNRM-CM3	Diurnal	July	0.809	0.753	29.1
CNRM-CM3	Semidiurnal	January	0.997	0.929	24.1
CNRM-CM3	Semidiurnal	July	1.021	0.890	24.6

* "Unmasked" means that comparison is made over the entire surface area of Earth. "Masked" means that land areas with elevation > 1 km are excluded from the comparison.

Figure Captions

Fig 1. Amplitudes in Pascals of (a) January diurnal harmonics and (b) January semidiurnal harmonics of surface or sea-level pressure variations from the Whole Atmosphere Community Climate Model (WACCM) version 1. Shown for each harmonic are (top) surface pressure variations, (middle) sea-level pressure variations, and (bottom) sea-level variations with overprinted gray shading for altitudes > 1 km. White areas indicate off-scale values, i.e. > 360 Pa.

Fig. 2. Amplitudes in Pascals of diurnal harmonics of (top) January sea-level pressure variations from two IPCC climate models, (bottom left) January surface pressure variations from WACCM version 3 and (bottom right) December – January – February surface pressure variations from observations. As in Fig. 1, gray shading indicates altitudes > 1 km for the sea-level pressure data; we excluded these areas from further analysis of the IPCC models.

Fig. 3. Same as Fig. 2 for the semidiurnal harmonics, but note different color scale.

Fig. 4. Local solar times of maximum near-surface pressure in the diurnal harmonics of (top) January sea-level pressure variations from two IPCC climate models, (bottom left)

January surface pressure variations from WACCM version 3 and (bottom right) December – January – February surface pressure variations from observations. The clock-face dial at the bottom of the figure gives the times.

Fig. 5. Same as Fig. 4 for the semidiurnal harmonics.

Fig. 6. Fourier-longitude amplitudes in Pascals vs. zonal wavenumber and latitude for the diurnal harmonics of (top) January sea-level pressure variations from two IPCC climate models, (bottom left) January surface pressure variations from WACCM version 3 and (bottom right) December – January – February surface pressure variations from observations.

Fig. 7. Same as Fig. 6 for the semidiurnal harmonics.

Fig. 8. (a) January and (b) July Fourier-longitude amplitude at the Equator vs. zonal wavenumber for (top) diurnal harmonics and (bottom) semidiurnal harmonics of all IPCC models providing data, WACCM-3, and observations. As in previous figures, WACCM output and observational data are surface pressure, available IPCC model output is sea-level pressure, and IPCC model output for altitudes > 1 km was excluded

from analysis. Blue-shaded insets show details of peaks in the vicinity of the migrating Fourier-component wavenumbers (red vertical lines).

Fig. 9. January and July migrating-tide phase vs. latitude for (top) diurnal harmonics and (bottom) semidiurnal harmonics of all IPCC models providing data and WACCM-3. As in previous figures, WACCM output and observational data are surface pressure, available IPCC model output is sea-level pressure, and IPCC model output for altitudes > 1 km was excluded from analysis.

Fig. 10. Global statistical comparison of model-simulated vs. observed tide amplitudes. Each point represents one model-simulated tide harmonic: semidiurnal for January (blue) and July (red); diurnal for January (brown) and July (green). Filled circles represent comparison of model-simulated sea level pressure tides vs. observed surface pressure tides, with elevations > 1 km omitted from the comparison. Asterisks represent comparison of model-simulated surface pressure tides (available only from WACCM) vs. observed surface-pressure tides with the comparison including all of Earth's surface. Three statistics are shown: (top row) globally averaged ratio of simulated / observed point values; (middle row) spatial correlation of simulated and observed; (bottom row) root-mean-square simulated – observed difference. The statistics are plotted as a function of both (left) the altitude of each model's top level and (right) the number of

model levels with significant solar radiation absorption by ozone (i.e., in the 30 – 70 km altitude range).

Fig. A1. The ratio of standard deviation to mean value over all Januarys in WACCM-3-simulated (top frame) diurnal and (bottom frame) semidiurnal tide amplitude, for years 1990 – 2000 inclusive.

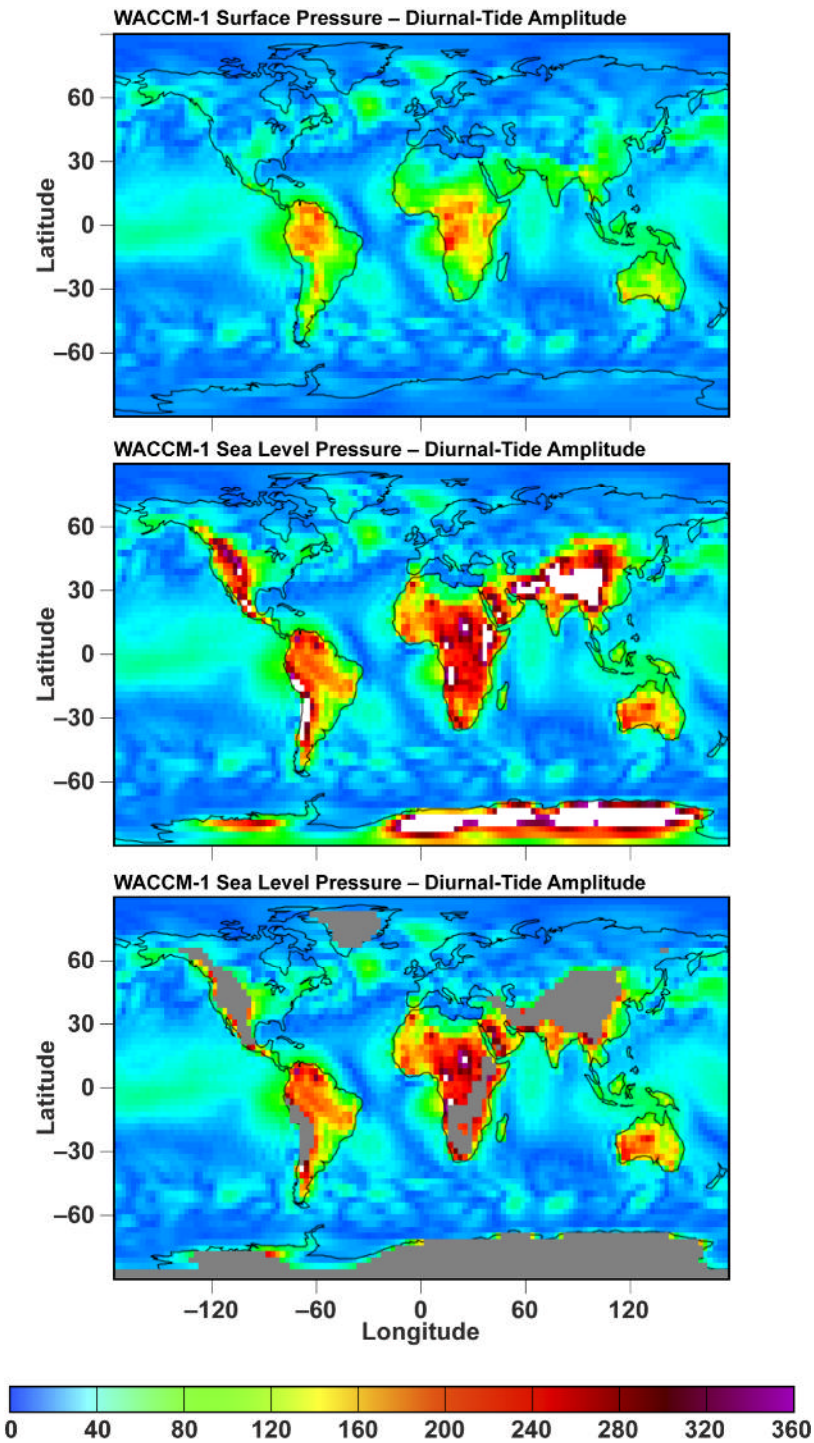

Fig 1a. Amplitudes in Pascals of January diurnal harmonics of surface or sea-level pressure variations from the Whole Atmosphere Community Climate Model (WACCM) version 1. Shown are (top) surface pressure variations, (middle) sea-level pressure variations, and (bottom) sea-level variations with overprinted gray shading for altitudes > 1 km. White areas indicate off-scale values, i.e. > 360 Pa.

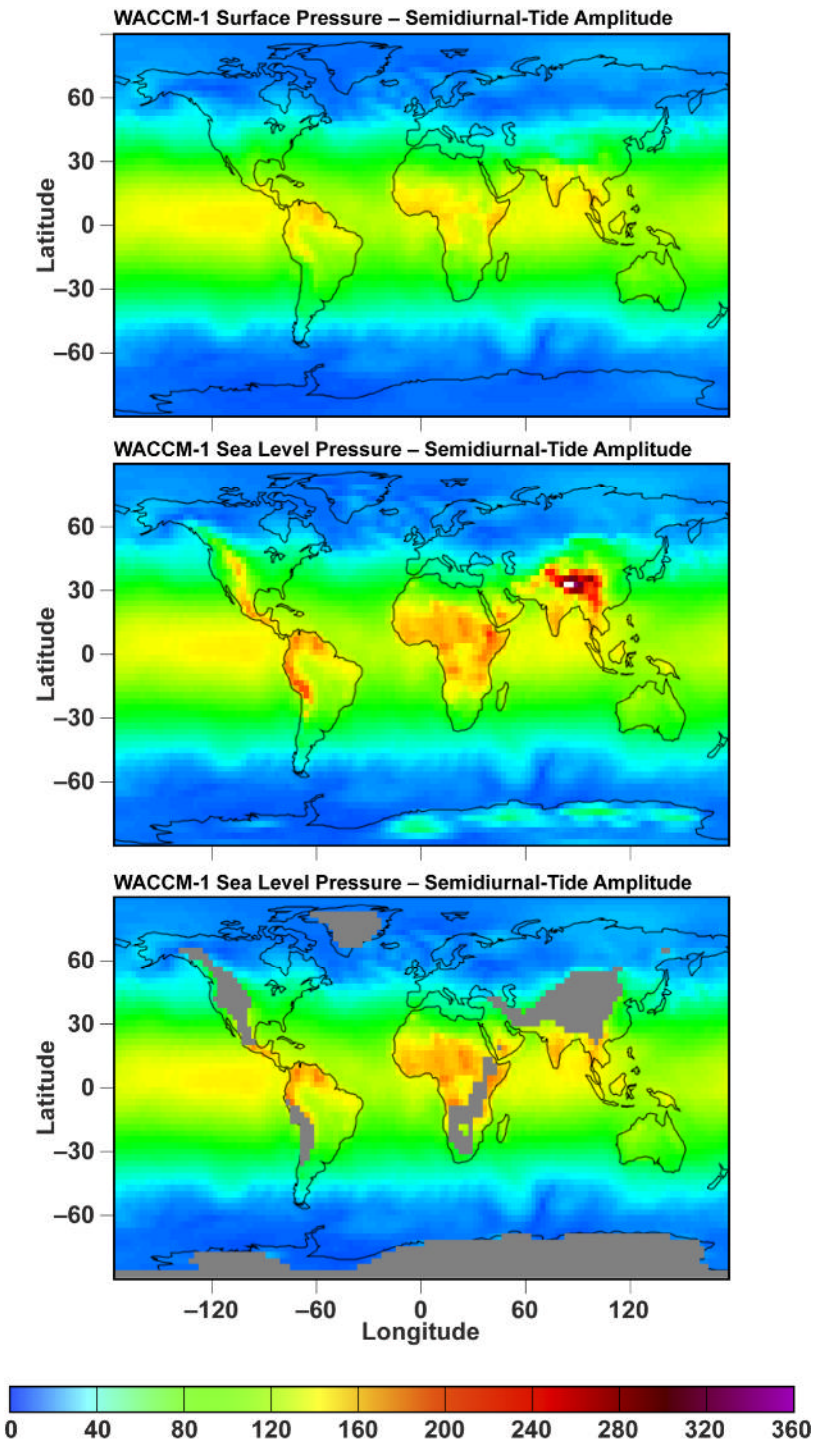

Fig 1b. Amplitudes in Pascals of January semidiurnal harmonics of surface or sea-level pressure variations from the Whole Atmosphere Community Climate Model (WACCM) version 1. Shown are (top) surface pressure variations, (middle) sea-level pressure variations, and (bottom) sea-level variations with overprinted gray shading for altitudes > 1 km. White areas indicate off-scale values, i.e. > 360 Pa.

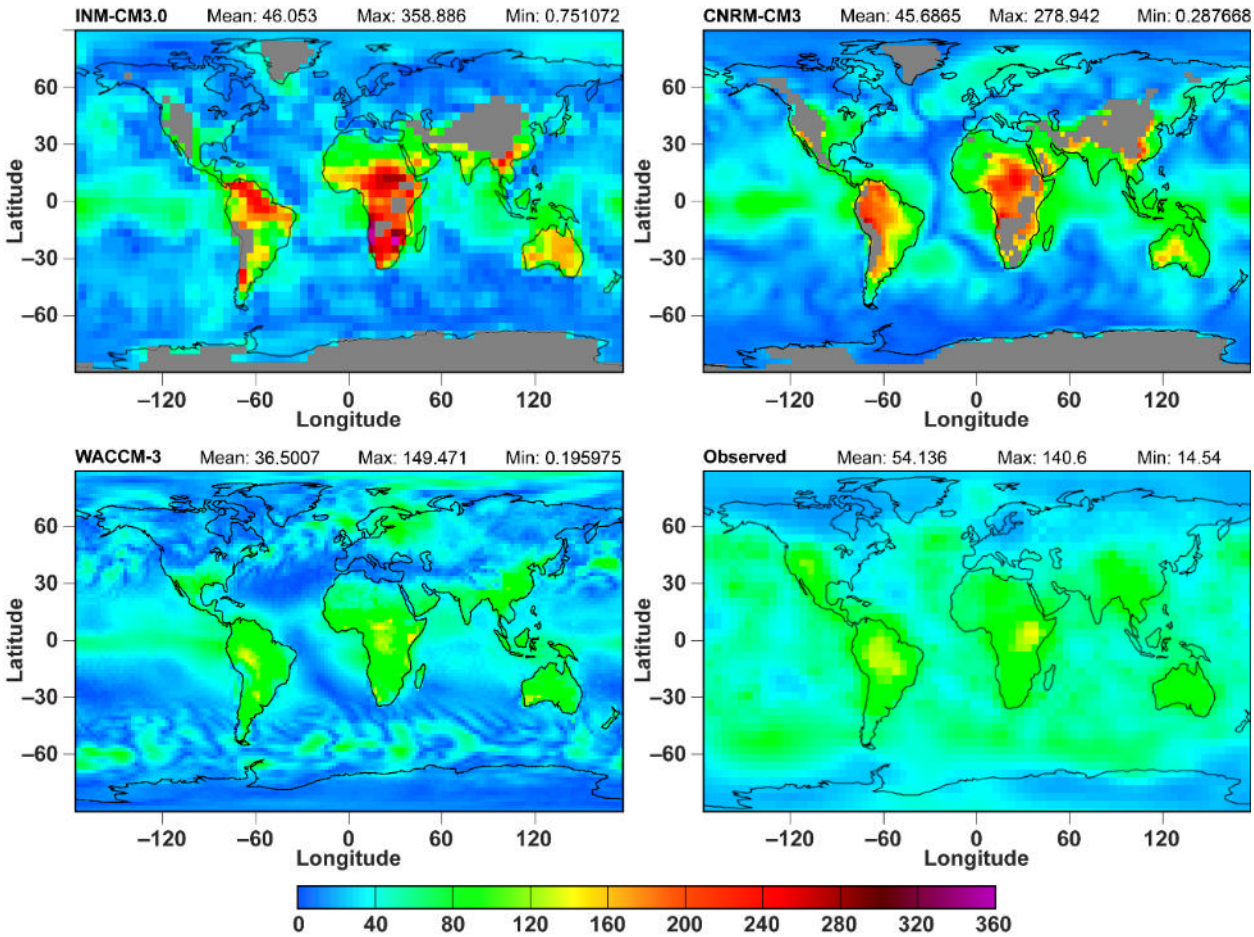

Fig. 2. Amplitudes in Pascals of diurnal harmonics of (top) January sea-level pressure variations from two IPCC climate models, (bottom left) January surface pressure variations from WACCM version 3 and (bottom right) December – January – February surface pressure variations from observations. As in Fig. 1, gray shading indicates altitudes > 1 km for the sea-level pressure data; we excluded these areas from further analysis of the IPCC models.

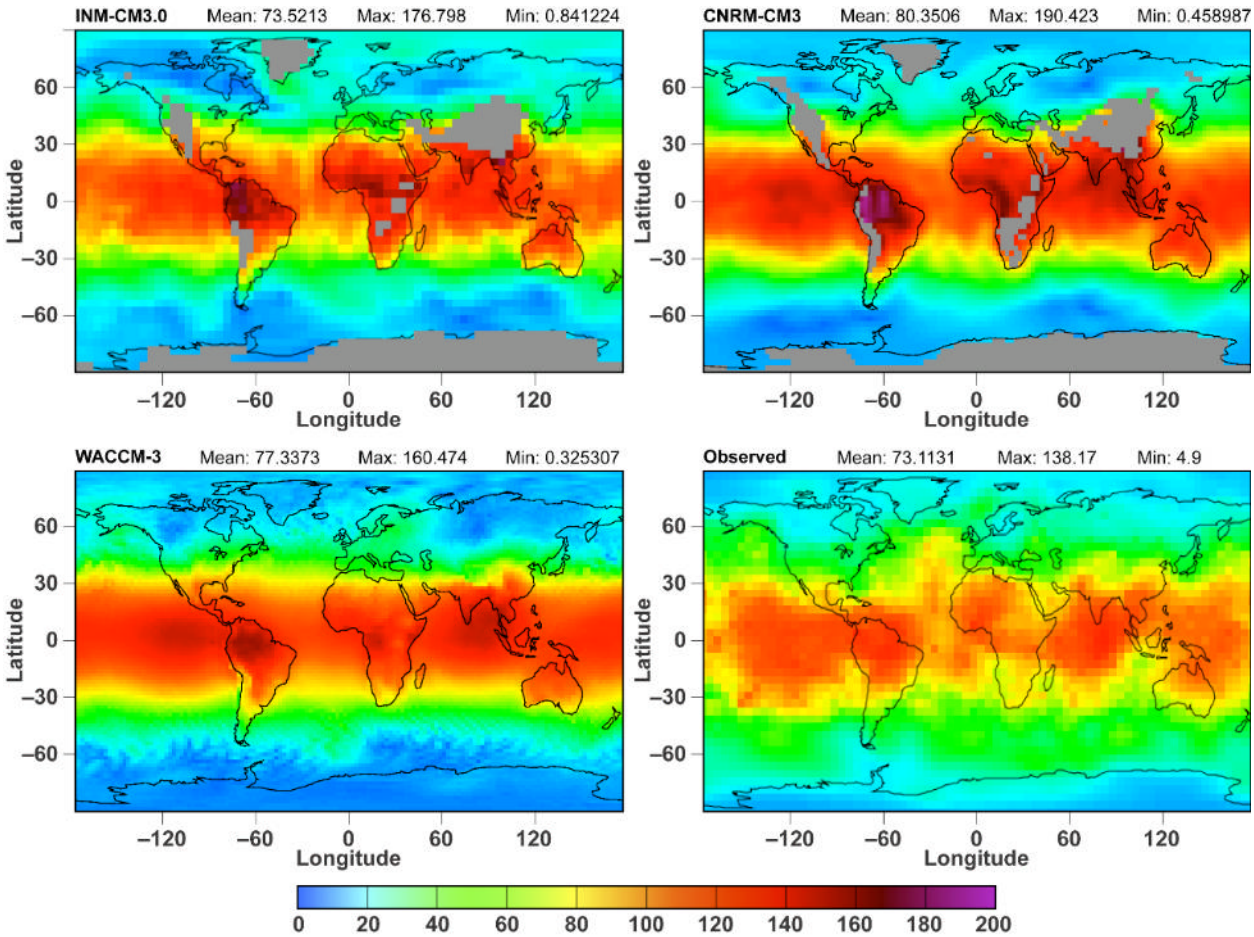

Fig. 3. Same as Fig. 2 for the semidiurnal harmonics, but note different color scale.

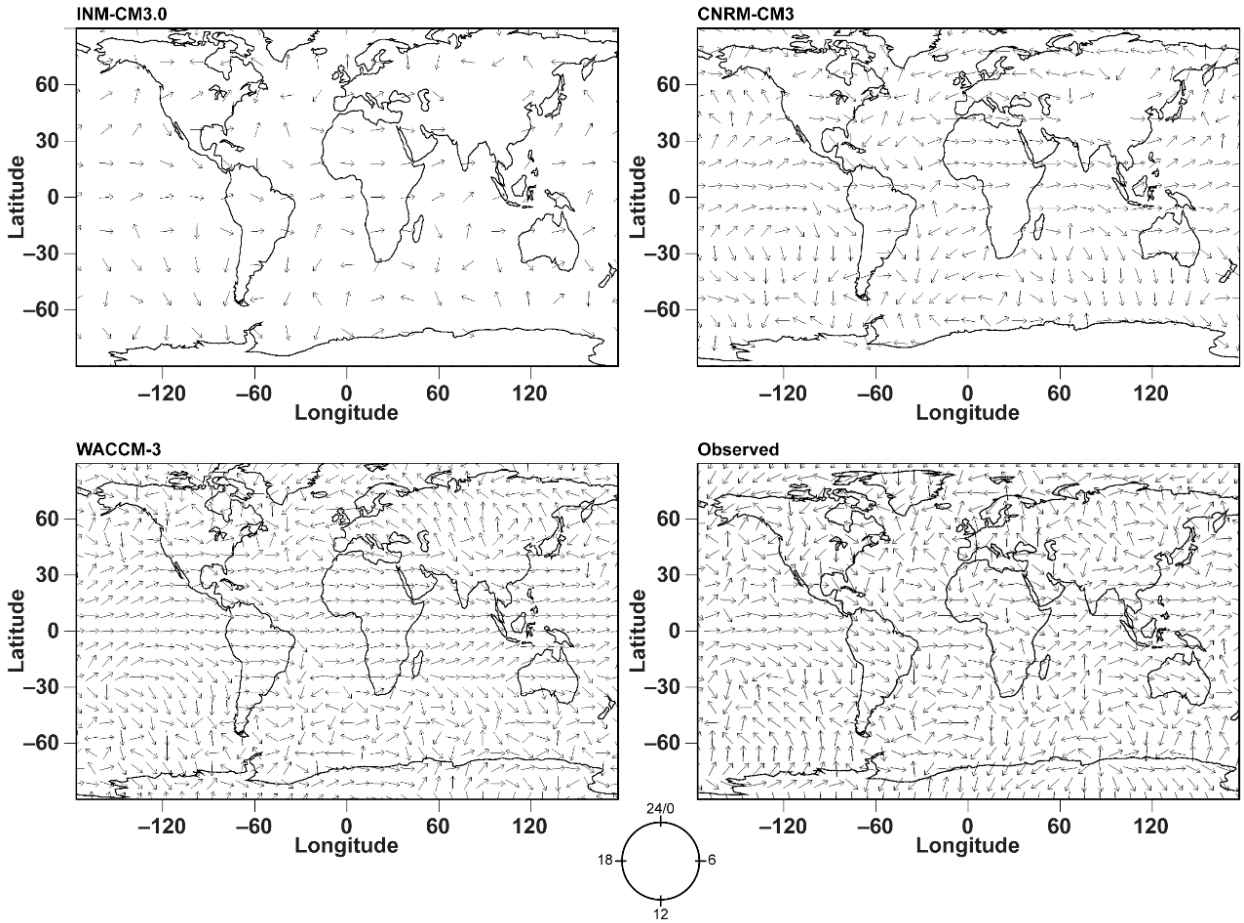

Fig. 4. Local solar times of maximum near-surface pressure in the diurnal harmonics of (top) January sea-level pressure variations from two IPCC climate models, (bottom left) January surface pressure variations from WACCM version 3 and (bottom right) December – January – February surface pressure variations from observations. The clock-face dial at the bottom of the figure gives the times.

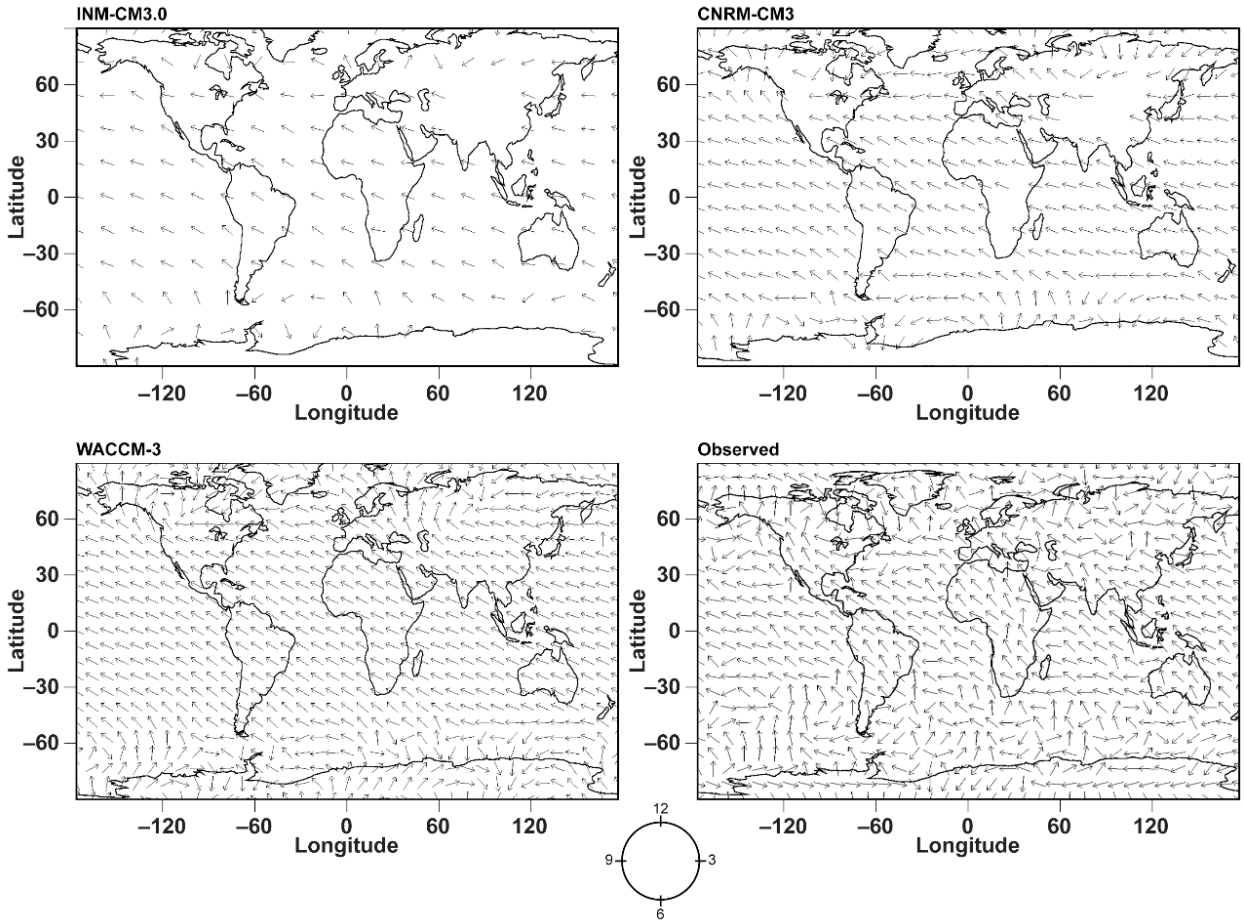

Fig. 5. Same as Fig. 4 for the semidiurnal harmonics.

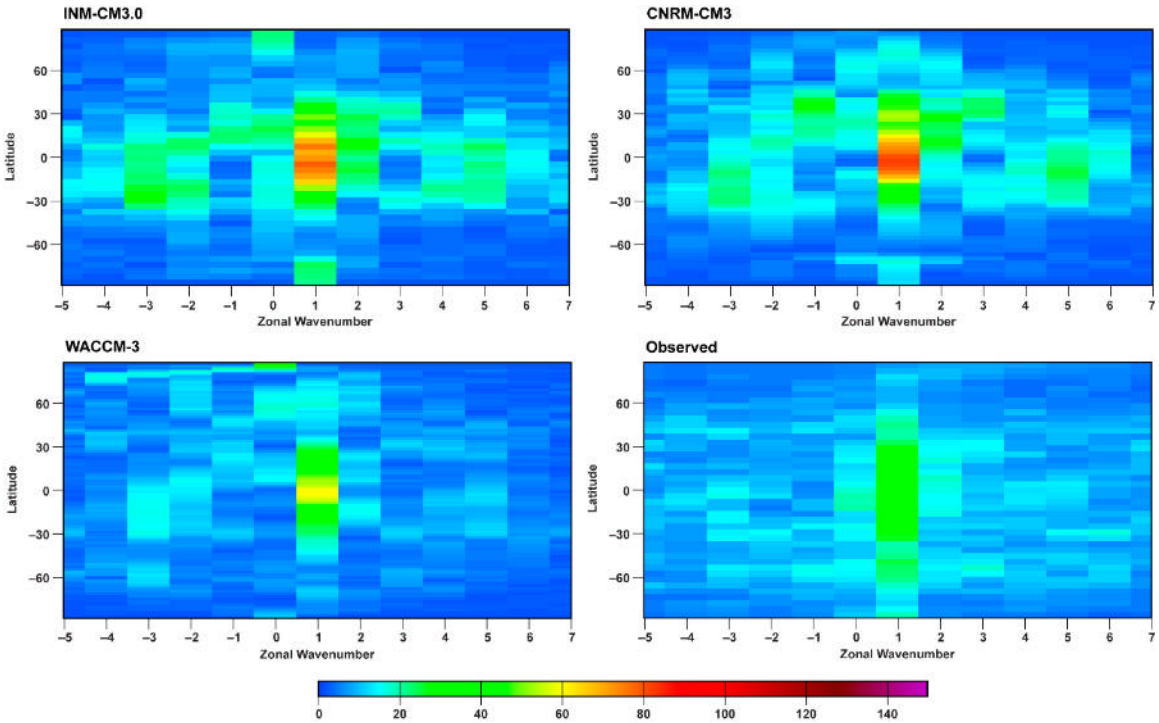

Fig. 6. Fourier-longitude amplitudes in Pascals vs. zonal wavenumber and latitude for the diurnal harmonics of (top) January sea-level pressure variations from two IPCC climate models, (bottom left) January surface pressure variations from WACCM version 3 and (bottom right) December – January – February surface pressure variations from observations.

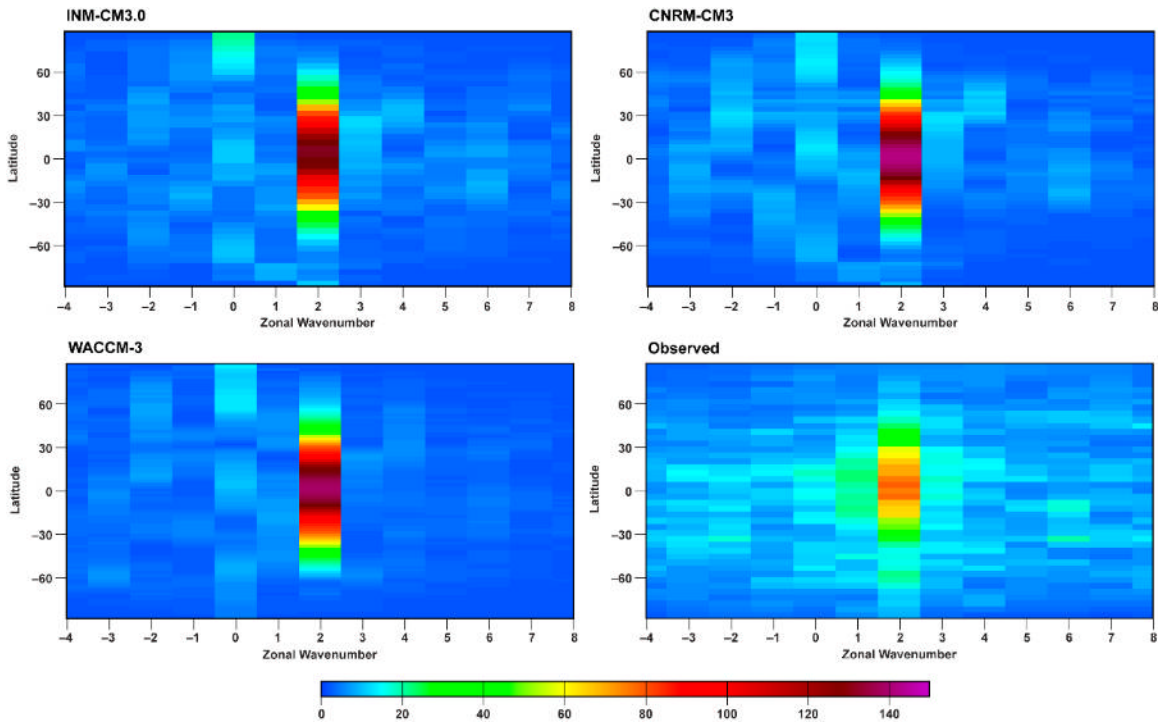

Fig. 7. Same as Fig. 6 for the semidiurnal harmonics.

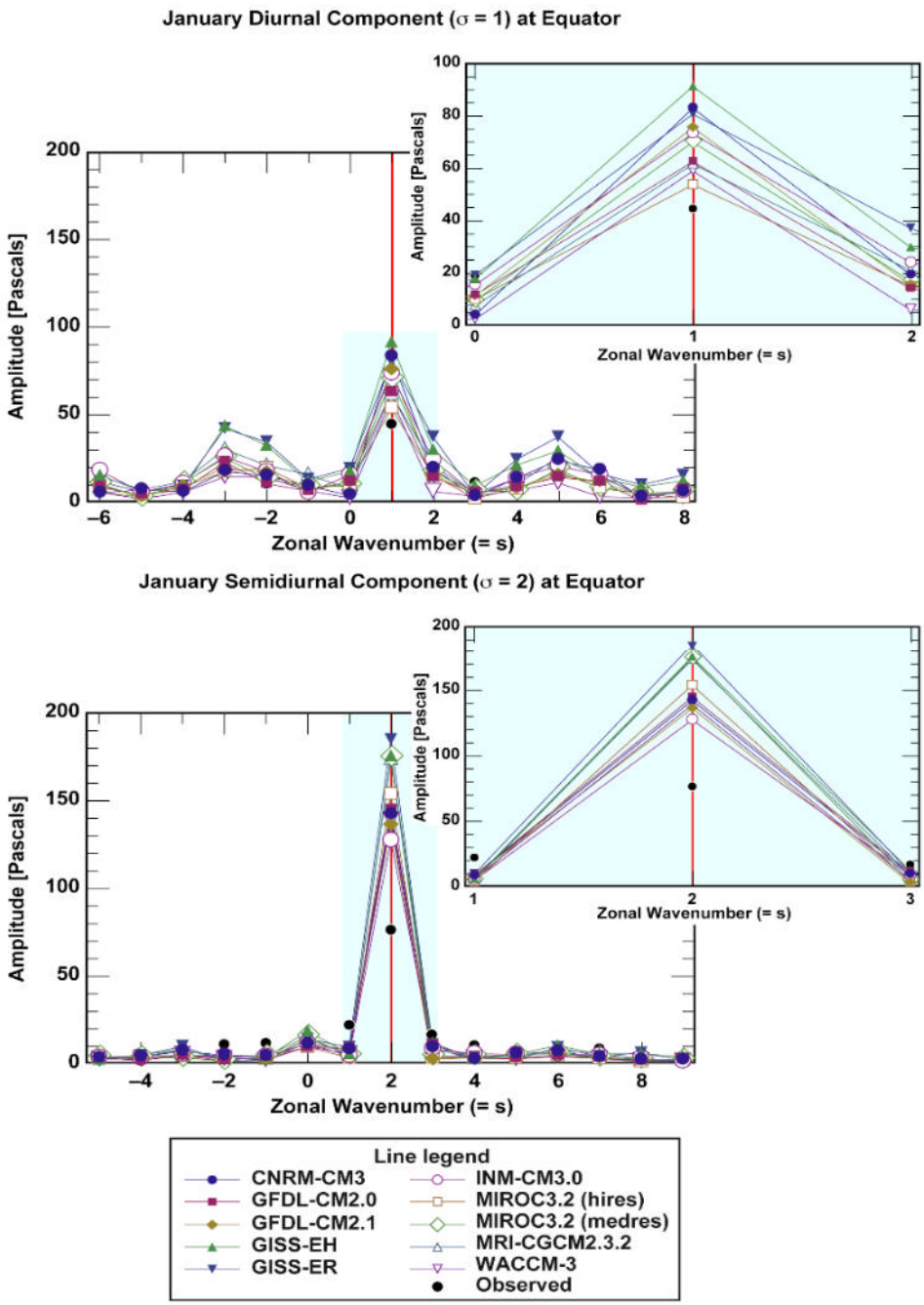

Fig. 8a. January Fourier-longitude amplitude at the Equator vs. zonal wavenumber for (top) diurnal harmonics and (bottom) semidiurnal harmonics of all IPCC models providing data, WACCM-3, and observations. As in previous figures, WACCM output and observational data are surface pressure, available IPCC model output is sea-level pressure, and IPCC model output for altitudes > 1 km was excluded from analysis. Blue-shaded insets show details of peaks in the vicinity of the migrating Fourier-component wavenumbers (red vertical lines).

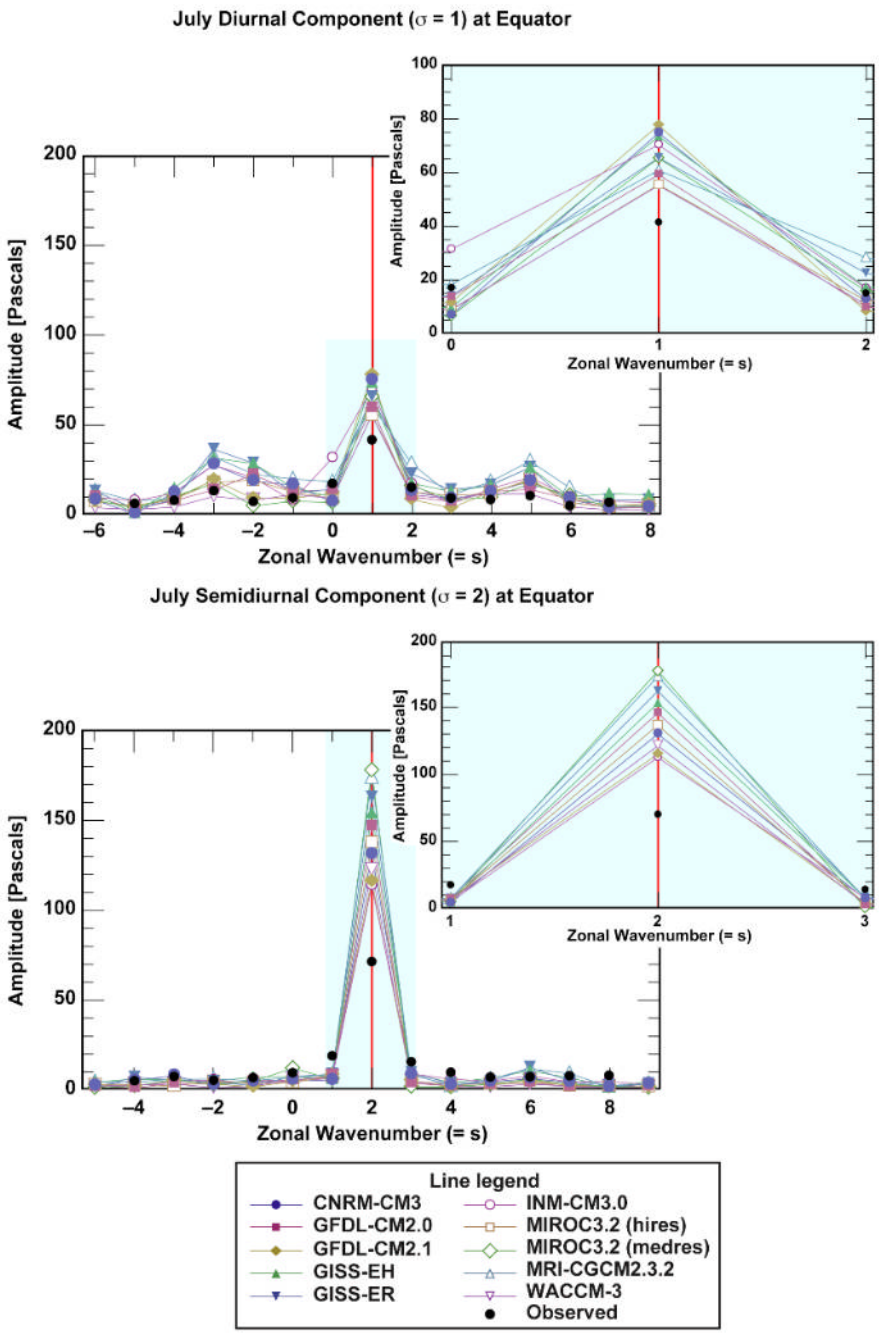

Fig. 8b. July Fourier-longitude amplitude at the Equator vs. zonal wavenumber for (top) diurnal harmonics and (bottom) semidiurnal harmonics of all IPCC models providing data, WACCM-3, and observations. As in previous figures, WACCM output and observational data are surface pressure, available IPCC model output is sea-level pressure, and IPCC model output for altitudes > 1 km was excluded from analysis. Blue-shaded insets show details of peaks in the vicinity of the migrating Fourier-component wavenumbers (red vertical lines).

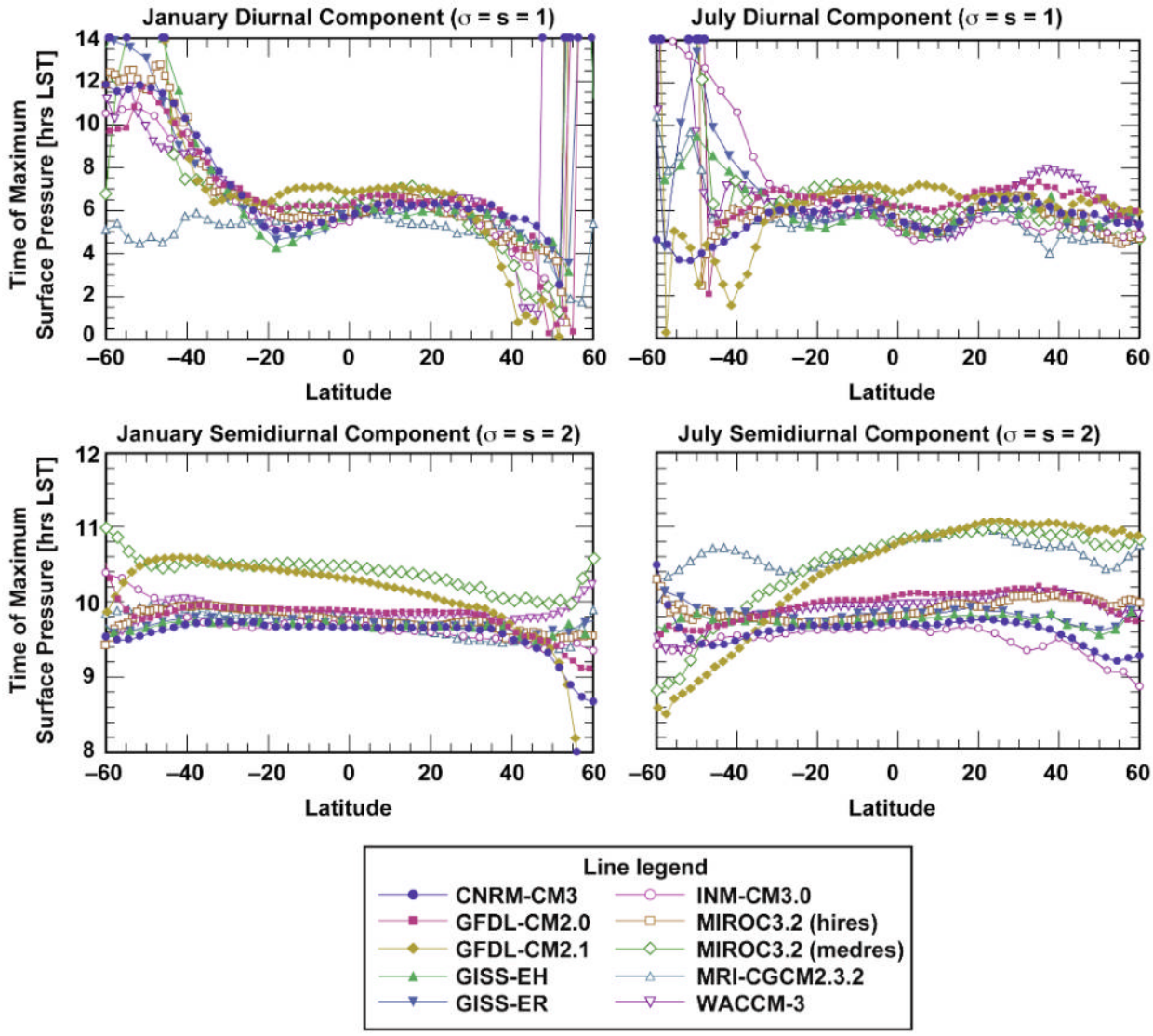

Fig. 9. January and July migrating-tide phase vs. latitude for (top) diurnal harmonics and (bottom) semidiurnal harmonics of all IPCC models providing data and WACCM-3. As in previous figures, WACCM output and observational data are surface pressure, available IPCC model output is sea-level pressure, and IPCC model output for altitudes > 1 km was excluded from analysis.

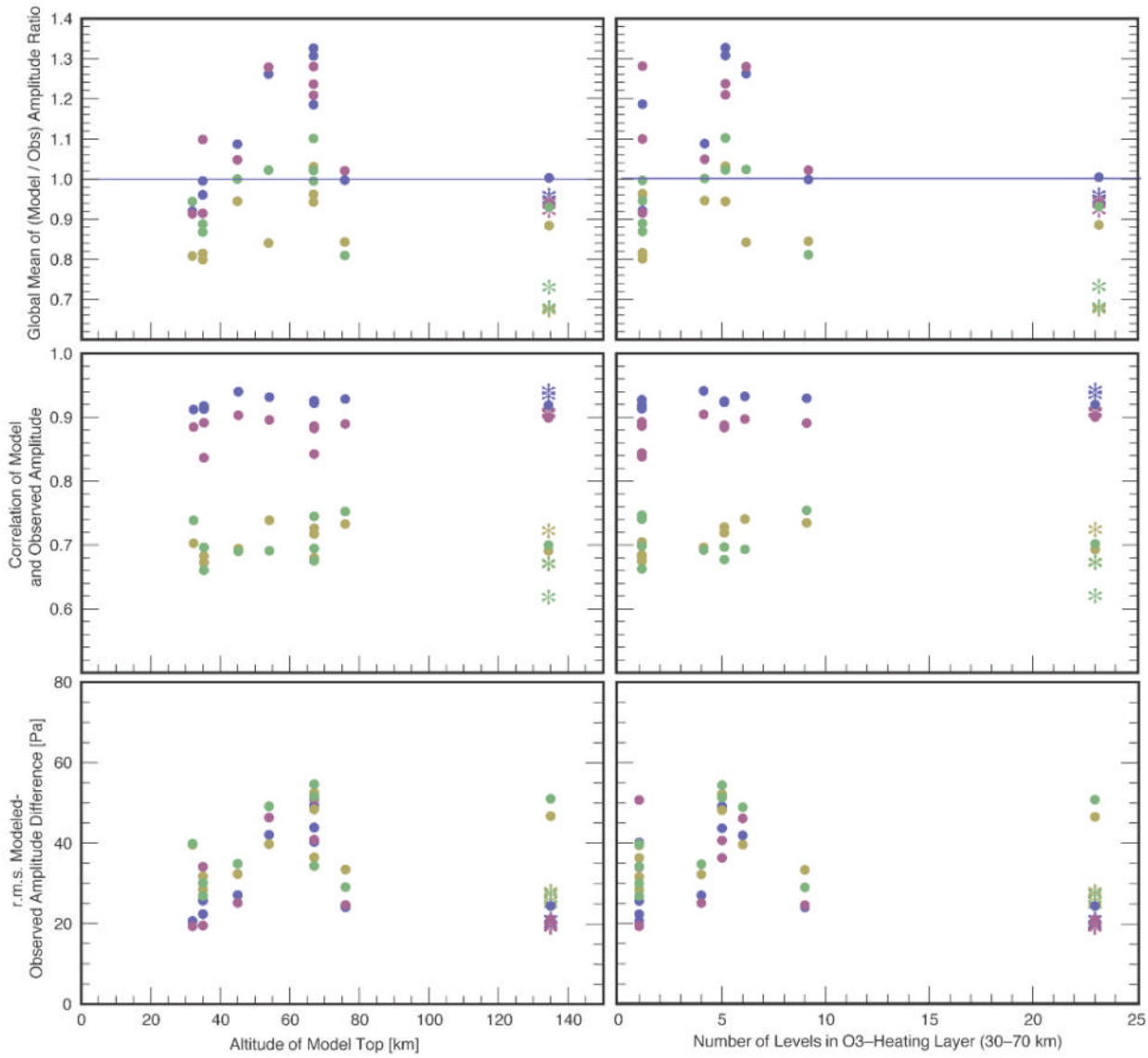

Fig. 10. Global statistical comparison of model-simulated vs. observed tide amplitudes. Each point represents one model-simulated tide harmonic: semidiurnal for January (blue) and July (red); diurnal for January (brown) and July (green). Filled circles represent comparison of model-simulated sea level pressure tides vs. observed surface pressure tides, with elevations > 1 km omitted from the comparison. Asterisks represent comparison of model-simulated surface pressure tides (available only from WACCM) vs. observed surface-pressure tides with the comparison including all of Earth's surface. Three statistics are shown: (top row) globally averaged ratio of simulated / observed point values; (middle row) spatial correlation of simulated and observed; (bottom row) root-mean-square simulated – observed difference. The statistics are plotted as a function of both (left) the altitude of each model's top level and (right) the number of model levels with significant solar radiation absorption by ozone (i.e., in the 30 – 70 km altitude range).

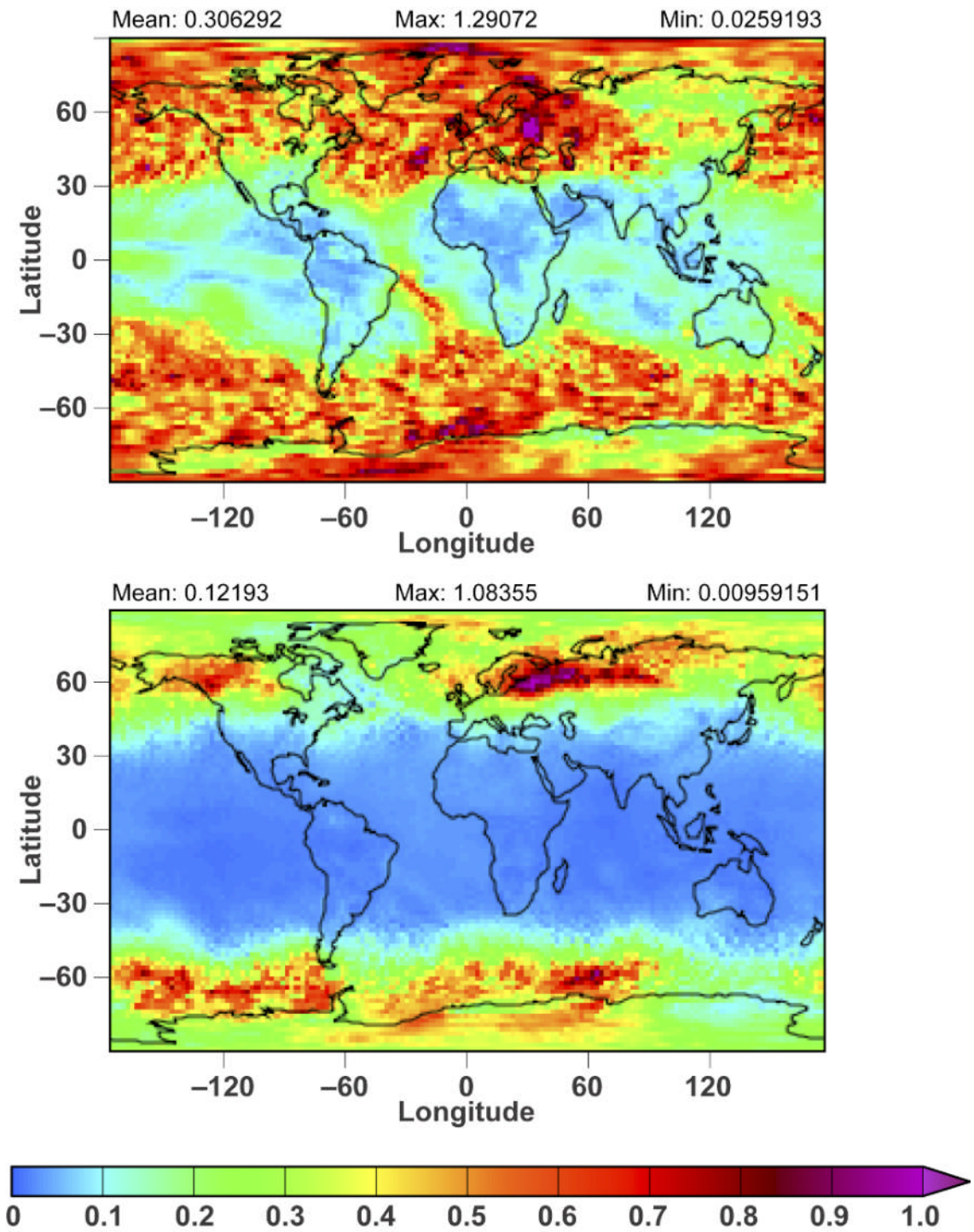

Fig. A1. The ratio of standard deviation to mean value over all Januarys in WACCM-3-simulated (top frame) diurnal and (bottom frame) semidiurnal tide amplitude, for years 1990 – 2000 inclusive.